Predicted thermoelectric properties of olivine-type Fe_2GeCh_4 (Ch = S, Se and Te)

2016 J. Phys.: Condens. Matter 28 025502

(http://iopscience.iop.org/0953-8984/28/2/025502)

IOP Publishing

Journal of Physics: Condensed Matter

J. Phys.: Condens. Matter **28** (2016) 025502 (12pp)

doi:10.1088/0953-8984/28/2/025502

Predicted thermoelectric properties of olivine-type Fe_2GeCh_4 (Ch = S, Se and Te)

Vijay Kumar Gudelli[1], V Kanchana[1] and G Vaitheeswaran[2]

[1] Department of Physics, Indian Institute of Technology Hyderabad, Ordnance Factory Estate, Yeddumailaram-502 205, Telangana, India
[2] Advanced Centre of Research in High Energy Materials (ACRHEM), University of Hyderabad, Prof C R Rao Road, Gachibowli, Hyderabad—500 046, Telangana, India

E-mail: kanchana@iith.ac.in

Received 14 July 2015, revised 12 November 2015
Accepted for publication 13 November 2015
Published 18 December 2015

Abstract

We present here the thermoelectric properties of olivine-type Fe_2GeCh_4 (Ch = S, Se and Te) using the linear augmented plane wave method based on first principles density functional calculations. The calculated transport properties using the semi-local Boltzmann transport equation reveal very high thermopower for both S and Se-based compounds compared to their Te counterparts. The main reason for this high thermopower is the quasi-flat nature of the bands at the valence and conduction band edges. The calculated thermopower of Fe_2GeS_4 is in good agreement with the experimental reports at room temperature, with the carrier concentration around 10^{18}–10^{19}cm^{-3}. All the investigated systems show an anisotropic nature in their electrical conductivity, resulting in a value less than the order of 10^2 along the *a*-axis compared to the *b*- and *c*-axes. Among the studied compounds, Fe_2GeS_4 and Fe_2GeSe_4 emerge as promising candidates with good thermoelectric performance.

Keywords: density functional theory, electronic structure, thermoelectric properties

(Some figures may appear in colour only in the online journal)

1. Introduction

Olivine minerals are well-known magnetic semiconducting materials. The magnetic semiconducting nature of the compounds generally finds applications in optoelectronic and magnetic devices [1]. The general formula for the olivine structure is A_2BC_4, and it mostly crystallises in an orthorhombic structure, where *A* is a transition metal, *B* represents *p*-orbital elements and Ch is the chalcogen. The arrangement of the atoms in the crystal is very closely packed and resembles a hexagonal close-packed arrangement. Among the olivine structures, Fe based olivines are well known because of their diverse magnetic nature at low and high temperatures [2–4]. Fe_2GeS_4 was found to possess weak a ferromagnetic nature up to 69 K, an anti-ferromagnetic nature between 69–143 K, and above this temperature it was reported to have a paramagnetic nature [5]. The ferromagnetic Curie temperature is around 149.9 K in Fe_2GeTe_4 [4]. A similar Fe-based olivine-type silicate, Fe_2SiO_4, is well known for its magnetic and optical properties [6]. The popularly known structure of pyrite FeS_2 with sulfur vacancy has a close relation to the olivine structure, which was explained extensively in the theoretical and experimental study by Yu *et al* [7], who also reported on the application of this material as a photovoltaic absorber. Following the above-mentioned work, an experimental study showed that nano-structured Fe_2GeS_4 can potentially be used as a photovoltaic material [8]. A similar study on highly crystalline nano-structured Fe_2GeS_4 was performed experimentally by Park and co-workers [9]. It is quite certain that there are interesting features that can be established in the structure of olivine other than the well-known magnetic properties. Apart from the magnetic studies and the recent photovoltaic studies, there are no further studies available for these materials. We are interested in studying the thermoelectric properties of the iron-based olivine structures of Fe_2GeCh_4 (Ch = S, Se and Te). This study mainly focuses on the prediction of the thermoelectric properties, where the motivation stems from the experimental study that showed that Fe_2SiS_4

and Fe_2GeS_4 possess good thermopower [10], enabling us to study the thermoelectric properties of the above-mentioned materials.

The performance of a thermoelectric (TE) material mainly depends on the figure of merit ZT, given by $ZT = S^2\sigma T/\kappa$. Here S, σ, κ and T refer to thermopower, electrical conductivity, thermal conductivity and absolute temperature, respectively. κ includes both the electronic κ_e and the lattice contributions κ_l, i.e. $\kappa = \kappa_e + \kappa_l$. For good thermoelectric materials, the typical value of ZT is around 1 and above. To achieve a figure of merit close to unity or above, we need materials to meet the requirement for high thermopower of around 200 μV K^{-1} and above, high electrical conductivity and low thermal conductivity. These are the challenges for current researchers searching for different classes of materials that achieve the conflicting properties of high thermopower, high electrical conductivity and low thermal conductivity. The successful thermoelectric materials that have a figure of merit close to unity include Bi_2Te_3, TAGS-85 (tellurium–antimony–germanium–silver) [11], filled skutterudites [12], PbTe/PbSe [13], etc. To explore the thermoelectric properties of iron-based olivine structures, we employed first principles-based electronic structure calculations using semi-classical Boltzmann transport equations. The rest of the paper is organised as follows: section 2 describes the methodology, section 3 presents the results and discussion and the conclusions are given in section 4.

2. Computational details

Total energy calculations based on first principles density functional theory (DFT) were performed using the full-potential linear augmented plane wave (FP-LAPW) method, as implemented in WIEN2k [14]. The total energies were obtained by solving the Kohn–Sham equations self-consistently. The self-consistent calculations included spin–orbit coupling (SOC). Since the calculations using standard local-density (LDA) or generalised gradient approximation (GGA) schemes for the exchange-correlation potential underestimate the band gaps of semiconductors, we used the Tran–Blaha modified Becke–Johnson [15] potential (TB-mBJ) [16] on top of GGA-Perdew–Burke–Ernzerhof (PBE) [17], which is quite good at reproducing the experimental band gaps. For k-space integrations, a $6 \times 11 \times 13$ k-mesh was used for Fe_2GeCh_4 in the Monkhorst–Pack scheme [18], resulting in 168 k-points in the irreducible part of the Brillouin zones for all the compounds. All the calculations were performed with an energy convergence criterion of 10^{-6} Ry per formula unit. The carrier concentration (both holes and electrons) and temperature (T) dependent thermoelectric properties like thermopower (S) and transport functions ($\frac{\sigma}{\tau}$; σ is the conductivity and τ is an inverse scattering rate) were computed using BOLTZTRAP [19] code, within the rigid band approximation (RBA)[20–22] and the constant scattering time (τ) approximation (CSTA) [23–25]. More details about RBA and CSTA can be found in [26] and references therein. The crystal structures were generated using VESTA [27] software and the charge density plots were generated with the help of the Xcrysden molecular structure visualization program [28].

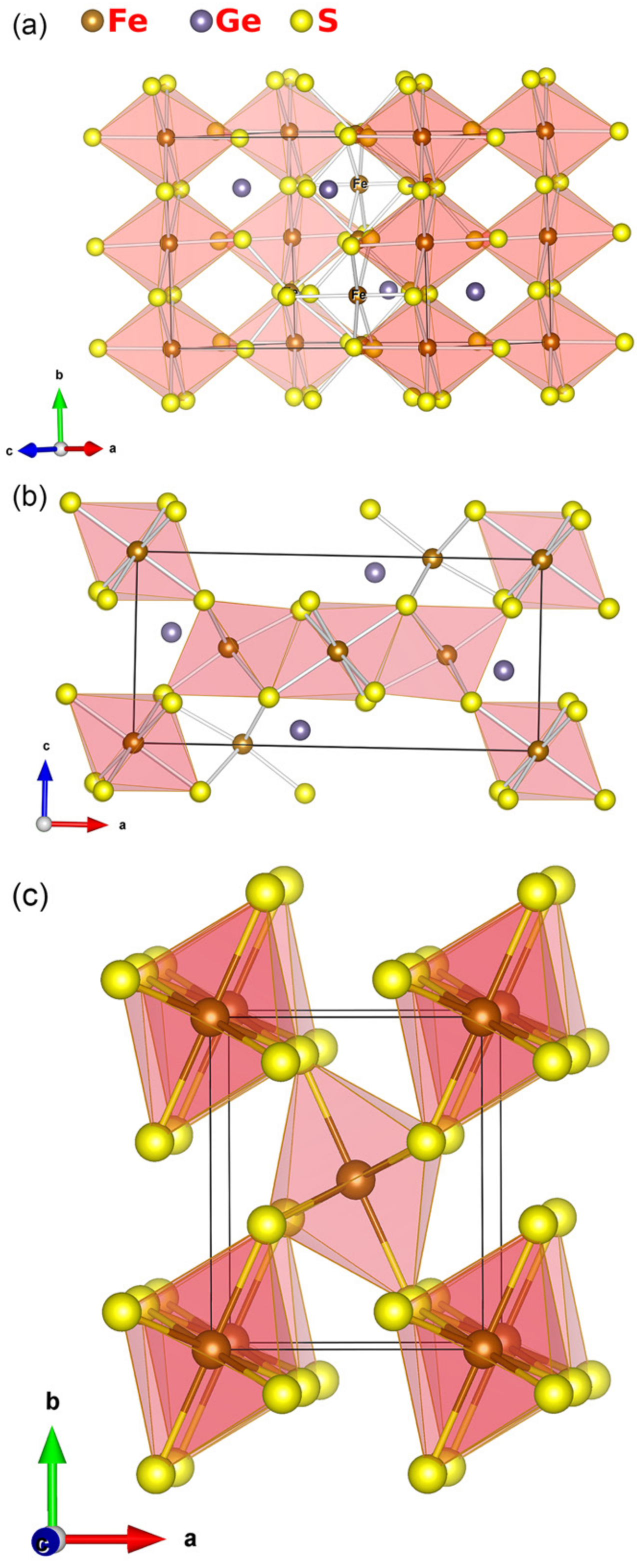

Figure 1. Crystal structure of (a) edge-sharing octahedra and (b) vertex-sharing octahedra of Fe_2GeS_4 compared with (c) marcasite FeS_2.

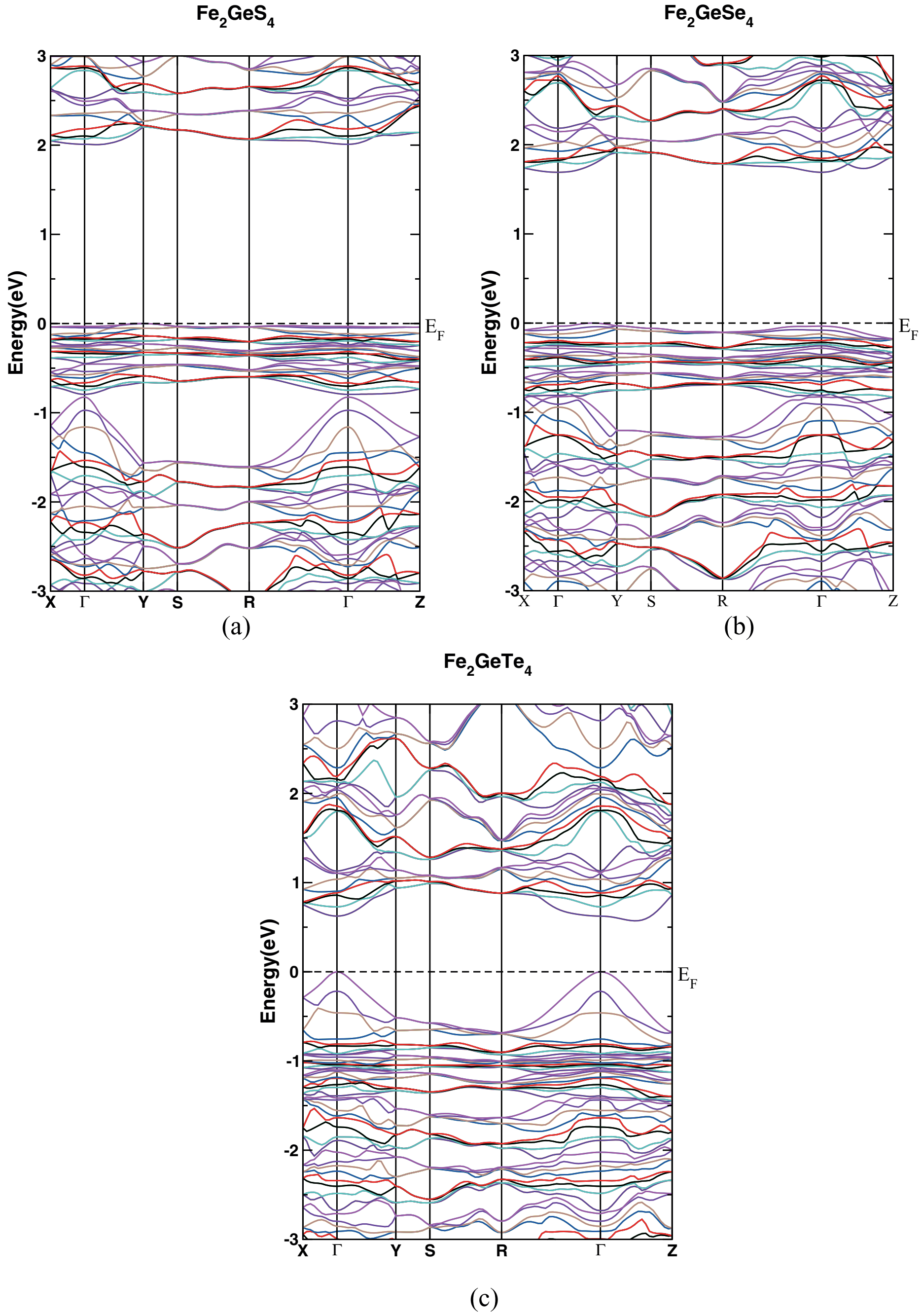

Figure 2. Calculated band structure of (a) Fe_2GeS_4, (b) Fe_2GeSe_4 and (c) Fe_2GeTe_4.

3. Results and discussion

3.1. Crystal structure and electronic structure of Fe_2GeCh_4

The olivine structure of Fe_2GeCh_4 is orthorhombic with space group *Pnma*. In this the cation Fe and the anion Ch forms a distorted octahedron $FeCh_6$. The Fe in Fe_2GeCh_4 has two independent Wyckoff positions, 4*a* and 4*c*. The coordination numbers of these two sites are similar, but are found to be different in the bond length between Fe–Ch and the orientation of the octahedron formed by them. The crystal structure of Fe_2GeS_4 is given in figure 1, which shows the edge and vertex sharing octahedra. The bond length of the Fe–S formed by Fe at the 4*a* site varies from 2.477 to 2.551 Å, which shows an average bond length of 2.494 Å and the distortion index of the octahedra is 0.011. In the case of Fe at the 4*c* site the variation of the bond length is from 2.449 to 2.629, with an average bond length of 2.539 Å and a distortion index of 0.024. This is clear evidence of the difference in the distortion of the octahedra formed by the two different Fe sites. We also observed that the distortion of the Fe at the 4*a* site is less than that for the 4*c* site Fe, which is very similar to that for Fe_2SiS_4 [10]. The two different orientations of the octahedra formed by Fe are important and differ in their contribution to the bands at the Fermi level, which is discussed in detail below. Earlier, Yu *et al* [7] explained the close relation

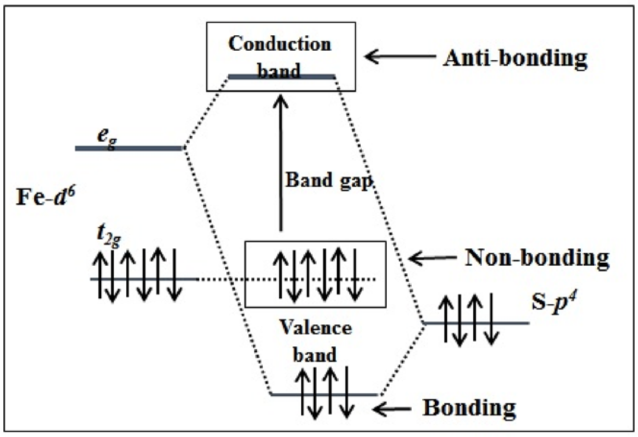

Figure 3. Schematic representation of octahedral crystal field splitting of Fe-*d* states in Fe_2GeCh_4.

of olivine-type Fe_2GeS_4 and Fe_2SiS_4 with pyrite FeS_2, and they also reported that these two compounds possess a similar absorption coefficient to pyrite. We found structural similarities between olivine and marcasite, which is a polymorphic phase of pyrite FeS_2. In both olivine and marcasite, we can see a distorted octahedron formed by Fe with sulfur. The edge sharing octahedra of olivine along the *b*-axis are also seen in marcasite, see figure 1, while the vertex sharing octahedra of olivine along the unit cell diagonal are also present in a similar direction of the unit cell diagonal of the marcasite. This shows that olivine-type structures have a very close relation with the polymorphic phases of marcasite and pyrite FeS_2. Our earlier work on the polymorphic phases of marcasite and pyrite showed a close relation between these two phases and also reported good thermoelectric properties for both phases [29]. This prompted us to study the thermoelectric properties of olivine structures further, and to compare the same with the polymorphic phases of FeS_2.

With the motivation mentioned above, we intend to study the thermoelectric properties through first principles electronic structure calculations. All the present calculations are performed at the experimental volume [30–32]. The electronic structure properties are carried out using the TB-mBJ exchange correlation functional. The band structure of all the compounds along the high symmetry directions is presented in figure 2. The corresponding energy gaps are found to be 2.01 eV for Fe_2GeS_4, 1.69 eV for Fe_2GeSe_4 and 0.6 eV for Fe_2GeTe_4. The experimentally reported band gap for Fe_2GeS_4 is 1.40 eV and the same group found it to be 1.36 eV with the GGA + U method [7]. In the present calculations, we find a slightly higher value with the TB-mBJ functional, which is also the case in other similar types of compounds with the same TB-mBJ functional [33]. The SOC has a significant effect in Fe_2GeTe_4 compared to Fe_2GeS_4 and Fe_2GeSe_4. This results in a degeneracy lift in Te-5*p* states of about 0.24 eV in Fe_2GeTe_4. The band structure of Fe_2GeS_4 and Fe_2GeSe_4 is quite similar, whereas Fe_2GeTe_4 is found to be different. The valence band maximum (VBM) is at *Y* and the conduction band minimum (CBM) is observed along $\Gamma - Y$ for Fe_2GeS_4, which results in an indirect band gap semiconductor, in agreement with earlier work [7, 10]. Similar behaviour for the indirect band gap is also seen in Fe_2GeSe_4 along $\Gamma - Y$ of VBM and at Γ in CBM. But Fe_2GeTe_4 is found to be a direct band gap semiconductor, with the VBM and CBM both occurring at Γ point. As indicated previously, the octahedra formed by Fe and Ch provide the hybridisation between Fe–Ch states. According to the octahedral crystal field splitting, the Fe-3*d* orbitals are divided into three filled t_{2g} and empty doublet e_g states. The crystal field splitting of Fe-3*d* is shown schematically in figure 3. The filled triplet states of t_{2g} contribute to the VBM as non-bonding states, with a very small contribution from Fe-$3d_{e_g}$ and S-3*p*. The empty doublet states of Fe-$3d_{e_g}$ interact with the chalcogen-*p* states and form the bonding states below the VBM. The higher energy states of Fe-$3d_{e_g}$ and chalcogen-*p* form the anti-bonding states that contribute to the CBM. The crystal field splitting is very similar to that of the prototype Rh_2ZnO_4 in the low spin state of the Rh [34, 35]. The Ge states reside much lower in the valence band.

The corresponding density of states (DOS) of all the compounds are shown in figure 4. From this figure, it is evident that at both the band edges, Fe-3*d* states are more dominant in all the compounds, but in the case of the valence band we also find that the chalcogen-*p* states make a small contribution (see figure 4(b)). The contribution of the Fe and S states at the VBM and CBM is very similar to that of the pyrite, since the Ge character in Fe_2GeS_4 is far below the valence band. This is evidence of the similarity between the olivine Fe_2GeS_4 and the pyrite FeS_2 [36, 37]. To further analyse the contribution of each element to the total DOS, we also plotted the orbital resolved DOS, i.e. the *m*-projected DOS of Fe_2GeS_4, which is shown in figures 4(c) and (d). The slight difference observed in the contribution of the two Fe states in the DOS at the Fermi level may be due to the different orientation of the $FeCh_6$ octahedra resulting in different bond lengths of Fe1 and Fe2 with sulfur, as mentioned above. The states below −1 eV in the valence band are due to the S-3*p* orbital. The crystal orbital overlap populations (COOP) analysis of Fe_2SiS_4 also showed a similar type of bonding [10]. We further investigated the nature of the bonding among the elemental species in Fe_2GeS_4 and the charge density plot is shown in figure 5. This shows that the bonding between Fe–S is a weak covalent bond, while Se–Ge form a strong covalent bond. The covalent bonding between Fe–S is stronger along the *b* and *c*-axes of Fe_2GeS_4 (see figures 5(b) and (c)), which might indicate a better flow of charge carriers along these two axes compared to the other axis *a*. This might be due to the presence of edge-sharing octahedra along the *b*-axis, which is layered through the *c*-axis, resulting in strong covalent bonding between Fe–S along the *b*- and *c*-axes, while along the *a*-axis the effect of edge and vertex sharing is weak, which eventually lowers the covalent bonding nature along this direction. In addition, it should be noted that the lattice parameter is larger along the *a*-axis, leading to reduced interaction and resulting in weak bonding along the respective crystallographic direction, which leads to a weak charge flow that results in low electrical conductivity along the *a*-axis, which is discussed below. From the band structure of Fe_2GeS_4 and Fe_2GeSe_4 it is evident that the dispersion of bands along the three crystallographic directions, i.e. $\Gamma - X$, $\Gamma - Y$ and $\Gamma - Z$,

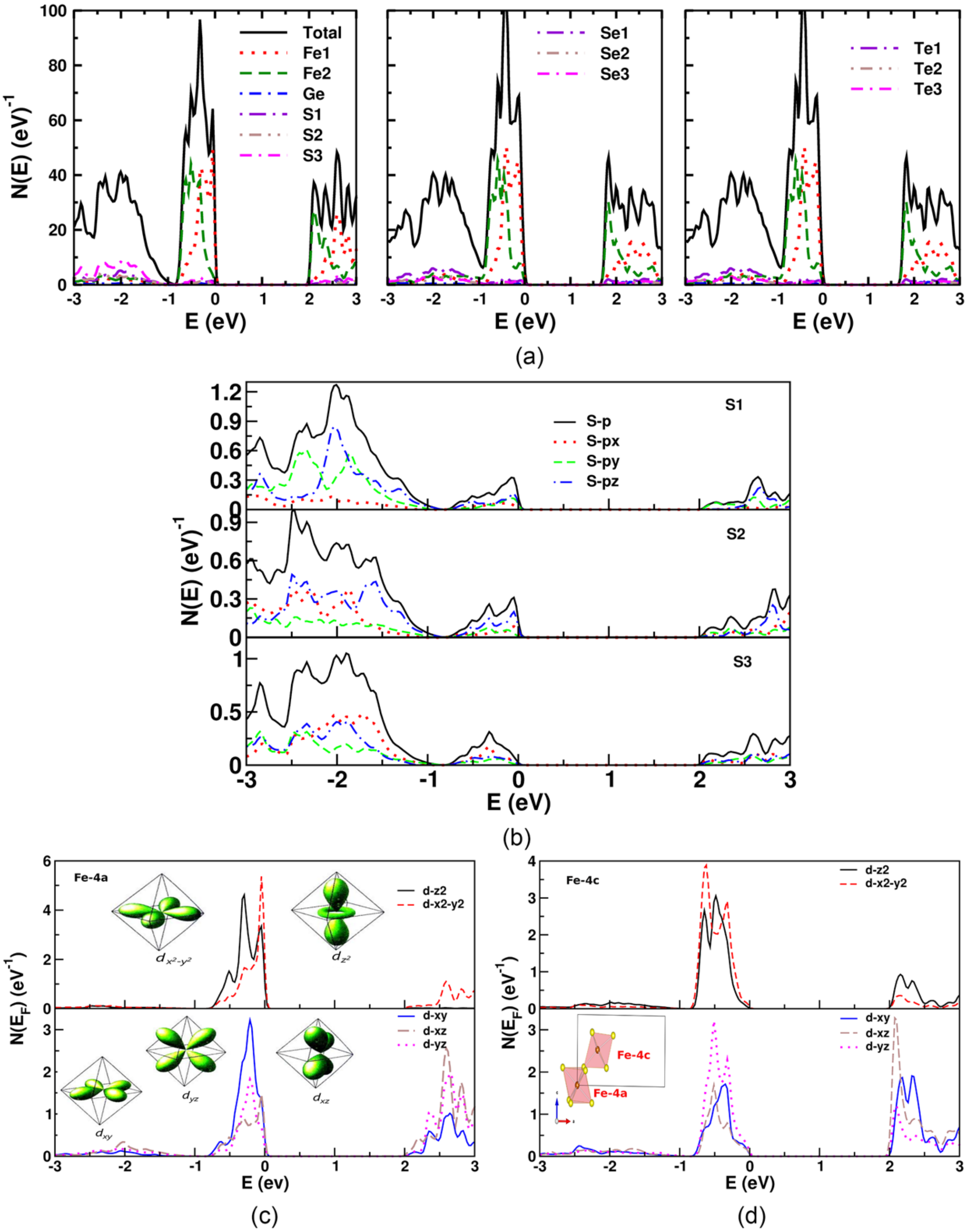

Figure 4. (a) Calculated DOS of Fe_2GeCh_4, and *m*-projected DOS for (b) S-*p*, (c) Fe1 at 4*a* and (d) Fe2 at 4*c* positions of Fe_2GeS_4.

are very flat in nature, which can result in a sharp increase in the DOS at the band edges. We observe an almost identical increase in DOS at both the edges in all the compounds, which might indicate favourable conditions for band-dependent properties such as thermopower for both the carriers.

The basis of this study is the prediction of the thermoelectric properties of Fe_2GeCh_4 as a function of carrier concentration at various temperatures. For this purpose one needs to study the effective mass of both the carriers at the band edges. We calculated the effective mass at the conduction and valence band edges by fitting the energy of the respective bands to a quadratic polynomial in the reciprocal lattice vector $\vec{k}$. The calculated effective mass of the bands along the $\Gamma - X$, $\Gamma - Y$ and $\Gamma - Z$ directions is shown in table 1. Lower values of the

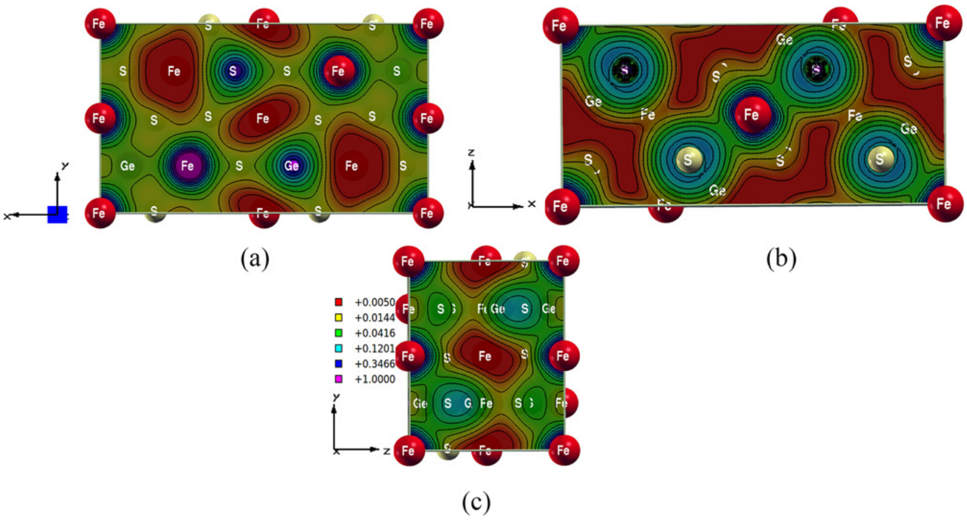

Figure 5. Calculated charge density density along the (a) *xy*, (b) *xz* and (c) *yz* planes of Fe_2GeS_4.

Table 1. The calculated effective mass of Fe_2GeCh_4 (Ch = S, Se, Te) in crystallographic directions of the Brillouin zone in units of electron rest mass.

Direction	Fe_2GeS_4	Fe_2GeSe_4	Fe_2GeTe_4
VBM			
$\Gamma - X$	6.80	3.11	0.29
$\Gamma - Y$	4.16	3.91	0.04
$\Gamma - Z$	4.21	4.18	0.53
CBM			
$\Gamma - X$	3.37	3.03	0.98
$\Gamma - Y$	3.39	3.02	0.91
$\Gamma - Z$	1.60	2.15	2.24

effective mass are observed for CBM compared to VBM. The effective mass values of both VBM and CBM (except along $\Gamma - Z$ of CBM) are found to decrease from sulfur to tellurium among the investigated compounds along the three directions mentioned above. The effective mass of the carriers of both Fe_2GeS_4 and Fe_2GeSe_4 are similar (slightly lower for Fe_2GeSe_4) because of the similar band structure of these two compounds, whereas in the case of Fe_2GeTe_4 we find the effective mass of the carriers to be lower, as a result of the highly dispersive bands along the specified directions, as mentioned above. The higher values for the effective mass of the carriers at both band edges might indicate high thermopower in Fe_2GeS_4 and Fe_2GeSe_4. With this preliminary idea, we calculated the transport properties for optimised doping levels of the carriers and this is discussed in the next section. The olivine Fe_2GeS_4 effective mass values are higher than those of marcasite and pyrite FeS_2, which shows that olivine-type minerals may have higher thermopower values than marcasite and pyrite, as seen in the present calculations and in the next section.

3.2. Thermoelectric properties of Fe_2GeCh_4

We now look at the thermoelectric properties of Fe_2GeCh_4. The uniform increase in DOS at both the edges suggests that these materials might show favourable thermoelectric properties for both the carrier concentrations. This allows us to calculate the carrier concentration-dependent thermoelectric properties, such as thermopower (S in μ V K^{-1}) and electrical conductivity scaled by relaxation time (σ/τ in $(\Omega\ \mathrm{m\ s})^{-1}$) using BoltzTrap code within the limit of RBA and CSTA, as mentioned in section 2, at various temperatures for both electrons and holes. As mentioned earlier, the olivine-type structure is non-cubic, and it is very important to analyse the direction-dependent thermoelectric properties, e.g. along the *a*, *b* and *c*-directions. From earlier studies it is evident that direction-dependent thermoelectric properties are very important because of the anisotropic nature of the systems [38–40]. For example, the delafossite type $PtCoO_2$ and $PdCoO_2$ revealed the importance of the anisotropic nature of the thermoelectric properties, where we can find a huge difference in the thermoelectric properties along the in-plane and out-of-plane directions [39]. Keeping the above consideration in mind, we calculated the direction-dependent thermoelectric properties such as S and σ/τ, which are presented in figures 6–8, for all the compounds for both the holes (n_h for holes) and electrons (n_e for electrons) as carriers. From the thermopower of all the compounds, we observed that there is no bipolar conduction seen in the case of Fe_2GeS_4 and Fe_2GeSe_4 (see figures 6(a) and 7(a)) because of the higher band gaps (>1 eV), whereas in Fe_2GeTe_4 (see figure 8(a)) we see bipolar conduction at higher concentrations in the case of holes and at lower concentrations in the case of electrons. Low band gap (0.6 eV) may be the reason for the bipolar conduction in Fe_2GeTe_4. From figure 6, it is clear that the thermopower of Fe_2GeS_4 varies from 850–250 μV K^{-1} for the optimum hole concentration of 10^{18}–10^{21} cm^{-3}, whereas for electrons, it is found to be 800–200 μV K^{-1}, and the range of the thermopower values is apparently very high at 300 K and 500 K in comparison with traditional thermoelectric materials [12, 13, 41–44]. For example, the commercially used thermoelectric material Bi_2Te_3 has a thermopower of 225 μV K^{-1} at room temperature [45], and we find the same thermopower value even at a high concentration around 10^{20} cm^{-3} in Fe_2GeS_4 at room temperature (the thermopower value is still higher at

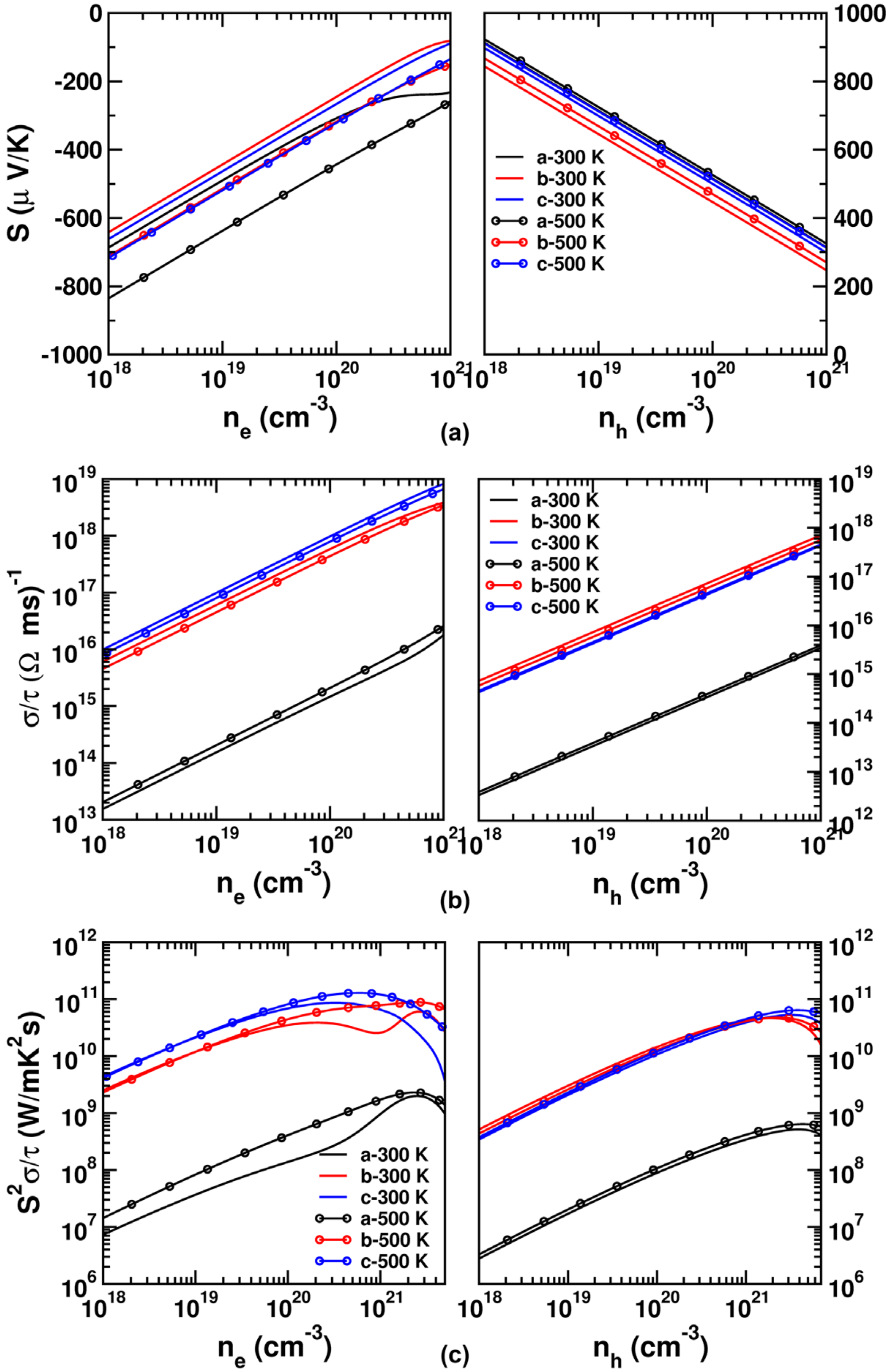

Figure 6. Calculated (a) thermopower, (b) electrical conductivity scaled by relaxation time and (c) power factor for Fe_2GeS_4.

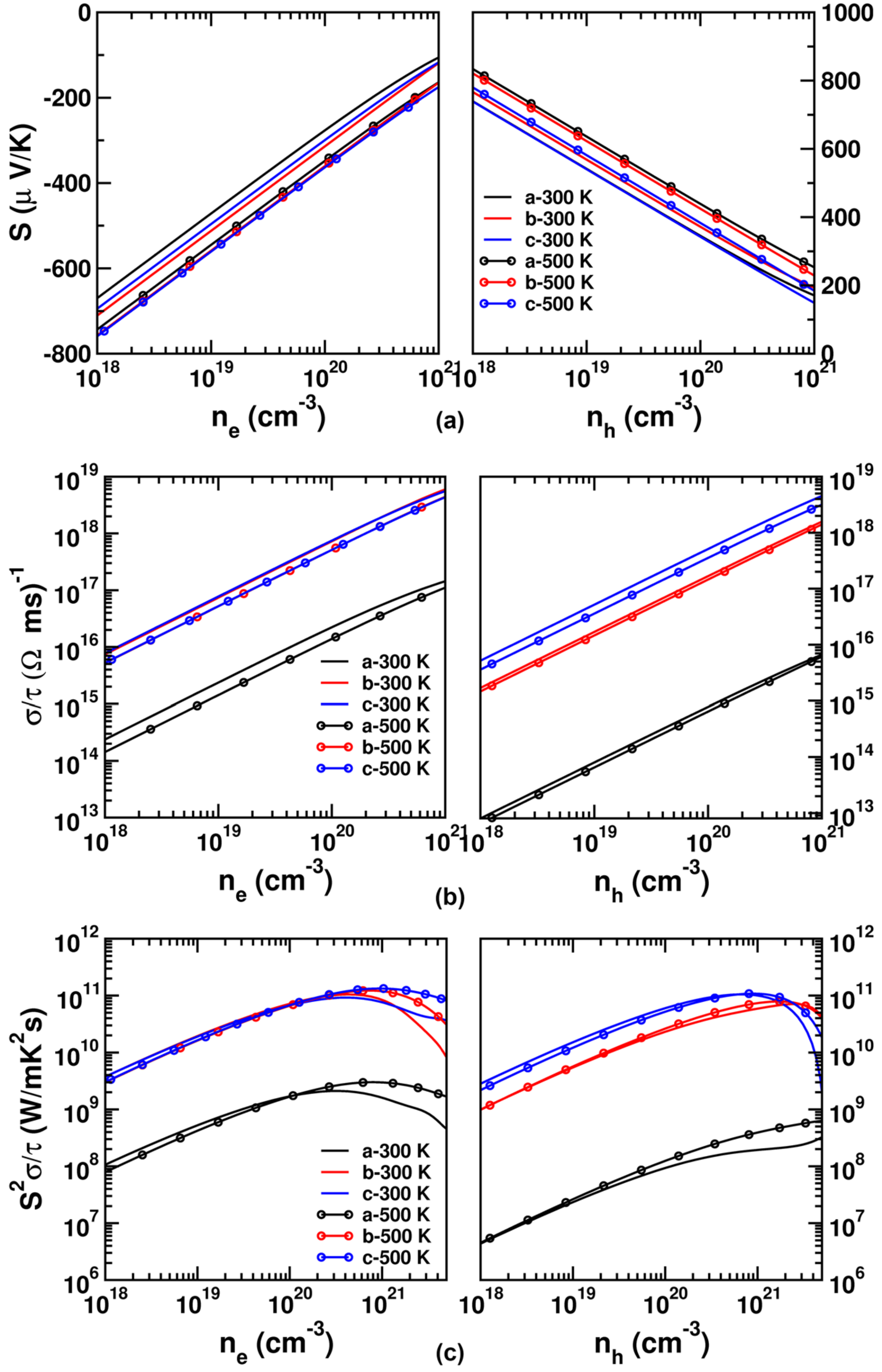

Figure 7. Calculated (a) thermopower, (b) electrical conductivity scaled by relaxation time and (c) power factor for Fe_2GeSe_4.

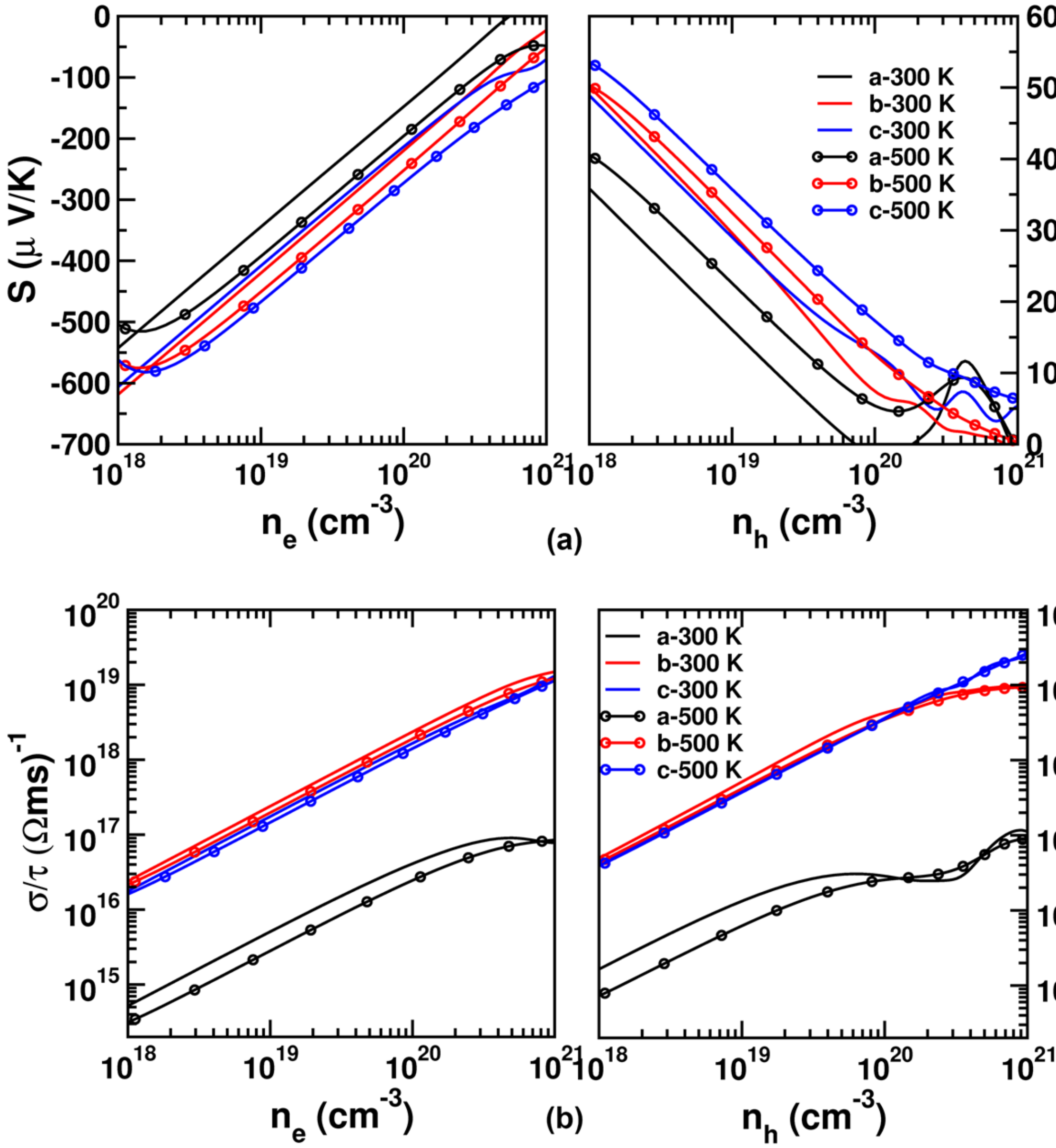

Figure 8. Calculated (a) thermopower and (b) electrical conductivity scaled by relaxation time for Fe_2GeTe_4.

lower concentrations). This shows that Fe_2GeS_4 might have a very high thermopower for both the carriers. In the case of Fe_2GeSe_4, the thermopower is found to be slightly lower compared to Fe_2GeS_4 because of the effective mass being smaller, as seen in table 1, but it is also shown to be more promising for both the carriers. In the case of Fe_2GeTe_4, we found lower thermopower values compared to the other two chalcogens, which was because of the lower values of the effective mass of the carriers in this compound. Thermopower was found to be below 550 μV K^{-1} at a hole concentration of 10^{18} cm^{-3}, whereas we found slightly higher values compared to holes in the case of electrons. However, there was bipolar conduction in the case of electrons at a lower concentration region. Anisotropy was seen in the thermopower in all the compounds along all three crystallographic axes. We also observed that the anisotropy increased as we moved down the chalcogens for both the carriers.

Earlier experiments on Fe_2GeS_4 showed a bulk thermopower of 750 μV K^{-1} at room temperature and in our study we found the same value at room temperature for the following concentrations: 1.14×10^{19} cm^{-3} along the *a*-axis, 9.31×10^{18} cm^{-3} along the *b*-axis and 5.15×10^{18} cm^{-3} along the *c*-axis for the holes [10]. The above-mentioned concentrations along the three directions can be achieved well within the experimental conditions for the semiconductors. In the case of the electrons we found the carrier concentration to be below 10^{18} cm^{-3} for the same thermopower of 750 μV K^{-1} at room temperature. The calculated thermopower of 750 μV K^{-1} for Fe_2GeS_4 at room temperature is in good agreement with the measured single crystal bulk thermopower of 750 μV K^{-1} at a concentration of around 5×10^{18} cm^{-3} [7]. This shows that the predicted thermopower values are in line with the experimental results. In comparison with the marcasite FeS_2 (∼300 μV K^{-1} @ 500 K), the thermopower of olivine-type Fe_2GeS_4 (∼460

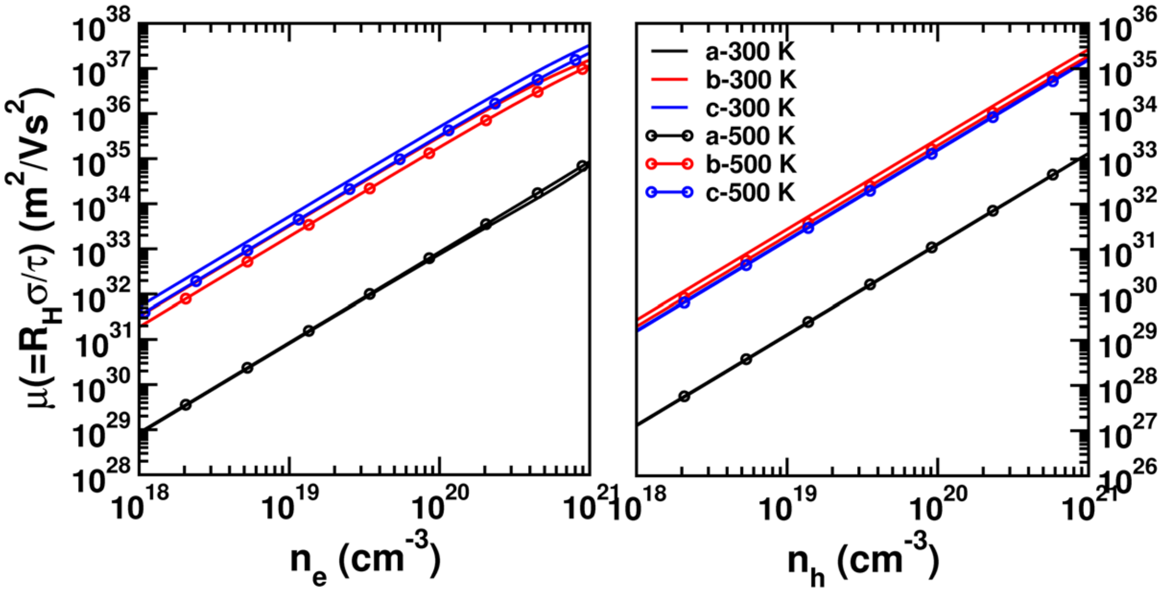

Figure 9. The calculated mobility scaled by the relaxation time of Fe_2GeS_4.

μV K^{-1} @ 500 K) has a higher value at a hole concentration of 10^{20} cm^{-3}. We find a similar thermopower value for pyrite FeS_2 ($\sim$500 μV K^{-1} @ 900 K) and olivine-type Fe_2GeS_4 ($\sim$500 μV K^{-1} @ 900 K) at the same concentration as mentioned above. This indicates that olivine can show better thermoelectric performance if it possess high electrical conductivity and low thermal conductivity. The electrical conductivity scaled by the relaxation time is discussed in the next section.

The electrical conductivity in all the compounds was found to be greater for electrons compared to holes. The electrical conductivity for the electrons was almost one order greater than that of the holes. We also observed a huge anisotropy along the *a*-axis compared to the *b* and *c*-axes. The σ/τ along the *a*-axis was almost two orders lower throughout the optimum concentrations for both the carriers for all the compounds. This might be due to the higher value of the lattice parameter '*a*' compared to '*b*' and '*c*' and also the weak covalent bonding nature along this direction compared to the other two axes, as mentioned earlier. A similar situation of lower electrical conductivity along the direction of the larger lattice parameter was found in the case of SnSe crystal [38]. As seen in the bonding, the interaction or the extent of hybridisation along the *a*-axis was also reduced. We found a significantly lower anisotropy between the *b* and *c*-axes in all the compounds. This eventually confirmed that the thermoelectric performance of the investigated compounds shows better applications along the *b* and *c*-axes compared to the *a*-axis. The electrical conductivity value was found to increase as we moved down the chalcogen group throughout the hole concentration. But in the case of electrons it was found to be a non-monotonic variation, where it decreased from Fe_2GeS_4 to Fe_2GeSe_4, followed by an increase in Fe_2GeTe_4 within the optimum electron concentration. The electrical conductivity of Fe_2GeTe_4 was found to be slightly higher compared to Fe_2GeS_4 in the case of electrons. But the bipolar nature of thermopower as seen in Fe_2GeTe_4 makes it unsuitable for good thermoelectric performance. This allows us to state that among the investigated olivine-type structures both Fe_2GeS_4 and Fe_2GeSe_4 emerge as good thermoelectric candidates for both the charge carriers. In order to understand the lower values along the *a*-direction, we further estimated the order of the mobility scaled by the relaxation time ($\mu = R_H \times \sigma/\tau$), and this is shown in figure 9. From this figure it is evident that the mobility of both carrier concentrations along the *a*-axis was very low compared to the other two axes, which resulted in electrical conductivity that was two orders lower along the *a*-axis. The lower value of the mobility along the *a*-axis is consistent with the charge flow mentioned in section 3.1.

We further studied the power factors ($S^2\sigma/\tau$) of Fe_2GeS_4 and Fe_2GeSe_4, as shown in figures 6(c) and 7(c). The power factor for electrons (above 10^{11} W m^{-1} K^{-2} s^{-1}) is slightly higher than that for the holes (below 10^{11} W m^{-1} K^{-2} s^{-1}) for Fe_2GeS_4, and this is because of the high electrical conductivity of electrons compared to the hole concentration of 10^{21} cm^{-3}. But in the case of Fe_2GeSe_4 we find nearly equal values for both electrons and holes ($\sim 10^{11}$ W m^{-1} K^{-2} s^{-1}). The calculated power factors for Fe_2GeS_4 and Fe_2GeSe_4 are found to be similar to those for the marcasite and pyrite structures of FeS_2 [29] and $FeSe_2$ [26]. We saw earlier that the thermopower value for olivine-type Fe_2GeS_4 is higher than that for marcasite and nearly equal to that for pyrite FeS_2, but we find lower power factor values because of the lower electrical conductivity of Fe_2GeS_4 ($\sim 0.6 \times 10^{17}(\Omega$ m s$)^{-1}$ @ 500 K and $\sim 0.5 \times 10^{17}(\Omega$ m s$)^{-1}$ @ 900 K) compared to marcasite ($\sim 1 \times 10^{18}$ (Ω m s$)^{-1}$ @ 500 K) and pyrite ($\sim 1 \times 10^{17}(\Omega$ m s$)^{-1}$ @ 900 K) (all the values are at 10^{20} cm^{-3} hole concentration). Even though the electrical conductivity of olivine is lower, its power factor is almost comparable with that of pyrite FeS_2, which implies that one needs to improve the electrical conductivity of olivine to obtain better TE performance. In general, we find the olivine-type Fe_2GeS_4 and Fe_2GeSe_4 to be good thermoelectric candidates along the crystallographic directions of the *b* and *c*-axes.

Overall, the less dispersive bands along the high symmetry directions are responsible for the higher thermopower in olivine Fe_2GeS_4 and Fe_2GeSe_4. We find a thermopower of above 300 μV K^{-1} at 300 K and 500 K at a concentration of 10^{20} cm^{-3} in both the compounds. These higher thermopower values, together with the assumption that these materials might possess low thermal conductivity, can certainly lead to good thermoelectric performance. As suggested by Tritt *et al*, the minimum thermopower a material should possess to have a $ZT \approx 1$ in the considerable range of around 160–225 μV K^{-1}, assuming zero lattice thermal conductivity [45]. In the present case, we find that the thermopower is high in both Fe_2GeS_4 and Fe_2GeSe_4, even at the higher carrier concentration of 10^{20} cm^{-3} for both electrons and holes. Earlier studies on Fe_2GeS_4 show this compound to possess a high absorption coefficient ($\sim 10^5$ cm^{-1}) [7], which implies their use as a good photovoltaic absorber and is similar to that of the pyrite FeS_2. In this study we also find a better thermoelectric performance for Fe_2GeS_4 compared to marcasite and pyrite FeS_2. This allows us to state that olivine-type compounds can be used as an alternative energy source material for both thermoelectric and photovoltaic applications. We look forward to experiments that will validate the proposed nature of the solar thermoelectric behaviour of the investigated systems.

4. Conclusions

We present here the thermoelectric properties of olivine-type Fe_2GeCh_4 (Ch = S, Se and Te) based on the Boltzmann semi-classical transport equation using first principles calculations. The investigated thermoelectric properties showed that Fe_2GeS_4 and Fe_2GeSe_4 have a high thermopower above 300 μV K^{-1}, even at room temperature and above, which is unusual and can be placed in a different regime of the thermoelectric family. We found a good agreement between the calculated hole concentration and the experimental measured carrier concentration of Fe_2GeS_4 at room temperature. The other interesting feature of these materials is the negligible anisotropy in the thermopower for the above two compounds, while the electrical conductivity is two orders less along the *a*-axis compared with the other two axes, *b* and *c*. A bipolar thermoelectric nature is observed for Fe_2GeTe_4 because of the narrow band gap. The calculated thermopower of the olivine-type Fe_2GeCh_4 is found to be higher when compared with the marcasite and pyrite structures. Among the investigated systems Fe_2GeS_4 and Fe_2GeSe_4 are shown to have good thermoelectric properties, especially along the *b* and *c* axes, and this presents substantial scope for future investigations in order to improve TE performance.

Acknowledgment

VK and VKG would like to acknowledge IIT-Hyderabad for providing computational facilities. GV thanks the Center for Modelling Simulation and Design-University of Hyderabad (CMSD-UoH) for providing computational facilities. VKG would like to thank MHRD for a fellowship.

References

[1] Williardson R K and Beer A C 1988 Diluted magnetic semiconductors, *Semiconductors and Semimetals* ed J K Fundyna and J-Kossut vol 25 (New York: Academic) chapter 1
[2] Ericsson T, Holnyi K and Amcoff O 1997 *J. Phys.: Condens. Matter* **9** 3943
[3] Baron V, Amcoff O and Ericsson T 1999 *J. Magn. Magn. Mater.* **195** 81–92
[4] Quintero M, Ferrer D, Caldera D, Moreno E, Quintero E, Morocoima M, Grima P, Bocaranda P, Delgado G E and Henao J A 2009 *J. Alloys Compd.* **469** 4–8
[5] Junod A, Wang K-O, Triscone G and Larnarche G 1995 *J. Magn. Magn. Mater.* **146** 21–9
[6] Jiang X and Guo G Y 2004 *Phys. Rev.* B **69** 155108
[7] Yu L *et al* 2011 *Adv. Energy Mater.* **1** 748–53
[8] Fredrick S J and Prieto A L 2013 *J. Am. Chem. Soc.* **135** 18256–9
[9] Park B-I, Yu S, Hwang Y, Cho S-H, Lee J-S, Park C, Lee D-K and Lee S Y 2015 *J. Mater. Chem.* A **3** 2265–70
[10] Platt H A S 2010 Copper and iron chalcogenides for efficient solar absorption *Thesis* Oregon State University (http://hdl.handle.net/1957/15009)
[11] Hsu K F, Loo S, Guo F, Chen W, Dyck J S, Uher C, Hogan T, Polychroniadis E K and Kanatzidis M G 2004 *Science* **303** 818
[12] Sales B C, Mandrus D and Williams R K 1996 *Science* **272** 1325
[13] Pei Y, Shi X, LaLonde A, Wang H, Chen L and Snyder G J 2011 *Nature* **473** 66
[14] Blaha P, Schwarz K, Madsen G K H, Kvasnicka D and Luitz J 2001 *WIEN2K, An Augmented Plane Wave + Local Orbitals Program for Calculating Crystal Properties* (*Karlheinz Schwarz, Techn. Universität Wien, Austria*) www.wien2k.at/
[15] Becke A D and Johnson E R 2006 *J. Chem. Phys.* **124** 221101
[16] Tran F and Blaha P 2009 *Phys. Rev. Lett.* **102** 226401
[17] Perdew J P, Burke K and Ernzerhof M 1996 *Phys. Rev. Lett.* **77** 3865–8
[18] Monkhorst H J and Pack J D 1976 *Phys. Rev.* B **13** 5188–92
[19] Madsen G K H and Singh D J 2006 *Comput. Phys. Commun.* **175** 67–71
[20] Scheidemantel T J, Ambrosch-Draxl C, Thonhauser T, Badding J V and Sofo J O 2003 *Phys. Rev.* B **68** 125210
[21] Jodin L, Tobola J, Pécheur P, Scherrer H and Kaprzyk S 2004 *Phys. Rev.* B **70** 184207
[22] Chaput L, Pécheur P, Tobola J and Scherrer H 2005 *Phys. Rev.* B **72** 085126
[23] Ong K P, Singh D J and Wu P 2011 *Phys. Rev.* B **83** 115110
[24] Singh D J 2010 *Funct. Mater. Lett.* **3** 223–6
[25] Parker D and Singh D J 2012 *Phys. Rev.* B **85** 125209
[26] Gudelli V K, Kanchana V, Vaitheeswaran G, Valsakumar M C and Mahanti S D 2014 *RSC Adv.* **4** 9424–31
[27] Momma K and Izumi F 2011 *J. Appl. Crystallogr.* **44** 1272–6
[28] Kokalj A 2003 *Comput. Mater. Sci.* **28** 155
[29] Gudelli V K, Kanchana V, Appalakondaiah S, Vaitheeswaran G and Valsakumar M C 2013 *J. Phys. Chem.* C **117** 21120–31

[30] Vincent H, Bertuat E F, Baur W H and Shannon R D 1976 *Acta Cryst.* B **32** 1749–55
[31] Henao J A, Delgado J M and Quintero M 1998 *Powder Diffr.* **13** 196–201
[32] Delgado G E, Betancourt L, Mora A J, Contreras J E, Grima-Gallardo P and Quintero M 2010 *Chalcogenide Lett.* **7** 133–8 (http://www.chalcogen.ro/133_Delgado.pdf)
[33] Dixit H, Saniz R, Cottenier S, Lamoen D and Partoens B 2012 *J. Phys.: Condens. Matter* **24** 205503
[34] Nagaraja A R, Perry N H, Mason T O, Tang Y, Grayson M, Paudel T R, Lany S and Zunger A 2011 *J. Am. Ceram. Soc.* **95** 16
[35] Volnianska O and Boguslawski P 2013 *J. Appl. Phys.* **114** 033711
[36] Rosso K M, Becker U and Hochella M F Jr 1999 *Am. Mineral.* **84** 1535–48 (www.minsocam.org/msa/ammin/toc/Articles_Free/1999/Rosso_p1535-1548_99.pdf)
[37] Eyert V, Höck K-H, Fiechter S and Tributsch H 1998 *Phys. Rev.* B **57** 6350–59
[38] Zhao L-D, Lo S-H, Zhang Y, Sun H, Tan G, Uher C, Wolverton C, Dravid V P and Kanatzidis M G 2014 *Nature* **508** 373–7
[39] Ong K P, Singh D J and Wu P 2010 *Phy. Rev. Lett.* **104** 176601
[40] Gudelli V K, Kanchana V, Vaitheeswaran G, Svane A and Christensen N E 2013 *J. Appl. Phys.* **114** 223707
[41] Stordeur M and Khnberger W 1975 *Phys. Status Solidi* B **69** 377–87
[42] Testardi L R, Bierly J N Jr and Donahoe F J 1962 *J. Phys. Chem. Solids* **23** 1209–17
[43] Jeon H-W, Ha H-P, Hyun D-B and Shim J-D 1991 *J. Phys. Chem. Solids* **52** 579–85
[44] Plechcek T, Navrtil J, Hork J and Lotk P 2004 *Phil. Mag.* **84** 2217–28
[45] Tritt T M and Subramanian M A 2006 *MRS Bull.* **31** 188